19

Atomic Force Microscopy of Protein–Protein Interactions

Xiaohui Zhang, Felix Rico, Amy J. Xu, and Vincent T. Moy

Abstract Since its invention in 1986, the atomic force microscope (AFM) has emerged as a flexible and powerful tool for exploring a variety of biological processes, including cell adhesion, protein folding, and protein–protein interactions. This review focuses on the application of the AFM to studies of protein–protein interactions. It describes the commonly used methodologies and reviews the theoretical framework used to analyze single-molecule protein–protein unbinding measurements. Finally, the chapter summarizes recent progress in the field and shows that the AFM provides an excellent tool for probing interactions on the cell surface and for understanding the energy landscapes that govern the dynamics of protein interactions.

19.1. Introduction

In recent years, new technologies have been developed to directly measure the dynamic processes of biological interactions at high spatial and temporal resolutions. In particular, single-molecule approaches such as atomic force microscopy and optical tweezers, with their ultrahigh resolutions down to subnanometer and submicrosecond levels, have opened new avenues to measuring individual molecular interactions in real time (1,2). This chapter focuses mainly on the application of the atomic force microscope (AFM) (3,4), a widely used single-molecule tool, to the study of protein interactions.

Proper protein–protein interactions are essential to normal physiological function in biological systems (5). Until recently, studies of protein–protein interactions usually involved biochemical methods that determine binding affinities or rate constants. Although these bulk measurements offer averaged estimates of interaction rates and free energies, they often miss

X. Zhang • Institute of Biochemistry and Cell Biology, Shanghai Institutes for Biological Sciences, Chinese Academy of Sciences, 320 Yue Yang Road, Shanghai 200031, China
F. Rico, V. T. Moy • Department of Physiology and Biophysics, University of Miami Miller School of Medicine, 1600 NW 10th Avenue, Miami, FL 33136, USA
A. J. Xu • MD/PhD program, HMS-MIT Division of Health Sciences and Technology, Harvard Medical School, 25 Shattuck Street, Boston, MA 02115, USA

P. Hinterdorfer, A. van Oijen (eds.), *Handbook of Single-Molecule Biophysics*,
DOI 10.1007/978-0-387-76497-9_19,

important features of interaction dynamics that uncover various intermediate states or alternative reaction pathways. Single-molecule approaches, however, avoid the intrinsic ensemble average of bulk methods and make it possible to follow the trajectories of individual interacting molecules in real time (1,6). Single-molecule methods, therefore, have become better tools for understanding the structure of the energy landscape governing the association, dissociation, and intermediate states of protein interactions (2,7). Moreover, on the cell surface, external forces continuously stretch molecules. For example, traction forces induce the cell surface adhesion receptors to undergo cycles of adhesion and de-adhesion as the cells migrate (8). Conventional techniques cannot reveal the influence of these internal and external forces associated with protein–protein interactions (9). Now, however, by using such force-measuring single-molecule tools as the AFM, optical tweezers, and biomembrane force probe, one can directly measure the forces holding protein complexes together and can access the stresses and strains associated with these reactions (2). Although each method has its merits, this chapter only discusses the use of the AFM in measuring protein interactions.

19.2. AFM Experimentation

19.2.1. AFM Principles

The essential components of an AFM are the cantilever; the tip; the sample stage; the piezoelectric translator, which accurately displaces the sample stage or cantilever; and the optical deflection system, comprising a laser and a photodetector, which records the changes in cantilever deflection (Figure 19.1).

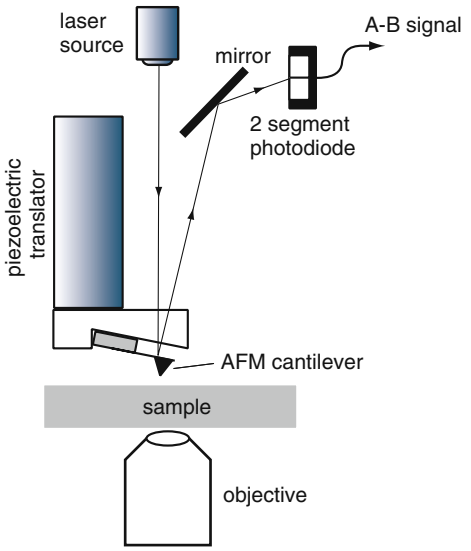

Figure 19.1. Schematic of the atomic force microscope (AFM). A beam of laser light is directed onto the cantilever and is reflected into a split photodiode. The difference (A-B) signal reports the forces exerted on the tip. Because the cantilever obeys Hooke's law for small displacements, the interaction force between the tip and the sample can be determined from the photodiode signal after a proper calibration of the spring constant of the cantilever.

Originally designed as an imaging tool (3), the AFM acquires topographic images by scanning the specimen with a flexible cantilever. In imaging mode, the AFM scans its tip, which is mounted to the end of a soft cantilever, over the specimen in the x, y plane (Figure 19.1). A piezoelectric element constantly corrects the position of the cantilever while scanning, to keep the deflection constant. Atomic-level resolution is acquired by translating the positioning of the cantilever into a topographic image of the sample surface.

Two formats are used to probe sample surfaces: a traditional design, which couples the sample stage to the movement of a three-dimensional piezoelectric translator, and a newer design, which instead scans the cantilever mounted on a piezo over a fixed sample (Figure 19.1). In the second approach, the AFM head is usually placed on the stage of an inverted optical microscope, allowing simultaneous acquisition of optical and AFM images. Therefore, the latter design is more feasible for working with living cells because it allows simultaneous visualization of cell shape and morphology.

The difference (A-B) signal from the photodetector reports the bending of the AFM cantilever due to forces exerted on the tip. The cantilever must be calibrated in order to translate its deflection into units of force. To this end, it is necessary to determine the spring constant of the cantilever, k_C. Different techniques are used for cantilever calibration (10) — measuring the cantilever's deflection (x) with the application of a constant known force (F) (11), or measuring of the cantilever's thermal oscillation resonant frequency (12). The most popular method for cantilever calibration, based on Hutter and Bechhoefer (12), treats the cantilever as a simple harmonic oscillator whose power spectrum of thermal fluctuations can be used to derive the spring constant. Since each vibration mode of the cantilever receives the thermal energy commensurate with one degree of freedom, $k_B T/2$, the measured variance of the cantilever's deflection $\langle x^2 \rangle$ can be used to calculate its spring constant, that is, $\frac{1}{2} k_B T = \frac{1}{2} k_C \langle x^2 \rangle$, where k_B and T are Boltzmann's constant and the absolute temperature, respectively.

19.2.2. AFM Measurement of Single-Molecule Interactions

The AFM can also be operated in force scan mode to measure interactions between two apposing surfaces at the single-molecule level. In this mode, a soft cantilever, usually with a spring constant of 10–100 mN/m and functionalized with a protein ligand, is positioned a few microns above a sample surface decorated with the molecule (such as a protein) of interest. The pyramid-shaped AFM tip, with a rounded apex of 10–50 nm in diameter, limits the contact between the two interacting surfaces so that it is possible to restrict the interaction between the surfaces to a single protein–protein bond (13). Figure 19.2 illustrates how unbinding experiments are performed.

When the cantilever is withdrawn from the surface, the unbinding forces of an individual protein–protein complex are determined experimentally from retraction curves by measuring the force jumps relative to the "zero-force" offset (Figure 19.2). In many experiments, force curves are obtained at cantilever velocities that can be as high as tens of microns per second. Due to the drag force exerted by the surrounding medium, the cantilever experiences a constant bending proportional to the applied velocity during its free approach and retraction. This hydrodynamic effect adds a systematic bias to the measured unbinding forces that has to be corrected when high velocities are applied. The drag force depends not only on the cantilever velocity and on the viscosity of the medium, which varies with temperature, but also on the geometry of the cantilever, the topography of the sample, and the relative separation between cantilever and sample (14,15). It is, thus, crucial to correct for this effect by systematically determining the viscous drag at each experimental condition. A straightforward

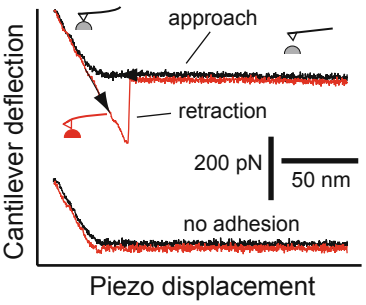

Figure 19.2. A representative unbinding trace. A representative atomic force microscope (AFM) force scan (i.e., optical signal vs. piezo displacement) under force scan mode. The two interacting surfaces are the AFM tip functionalized with streptavidin and an agarose bead with immobilized biotin. When the measurements started, the piezo first expanded and moved the agarose bead closer to the cantilever. Before the bead and cantilever touched, the deflection/force signal maintained a stable baseline level corresponding to "zero force." When the bead touched the cantilever, the cantilever bent upward, leading to a positive change of the deflection/force signal. The piezo ceased to expand when a preset compression force was reached (200 pN in this case). During the preset contact duration, the streptavidin and biotin had time to interact with one another. Adhesive contact created during this time was revealed by a downward deflection of the cantilever when the piezo started to contract and gradually moved the bead to its initial position. Further retraction movement of the bead resulted in a gradual increase of tension applied to the avidin–biotin bond(s) until the bond(s) were ruptured, indicated by a sharp vertical transition in the retraction trace, after which the cantilever returned to its original "zero-force" resting position.

approach to determining the viscous drag force is to measure the force shift just after the jump between the "zero force" values of the approach and retraction traces.

Using the force scan mode of an AFM, Lee et al. (16) and Florin et al. (13) directly measured the unbinding force of a single avidin–biotin interaction. Since the method was first reported in 1994, hundreds of different protein–protein interactions have been studied using this or similar methods. Table 19.1 provides a partial list of the unbinding forces and Bell–Evans model parameters of measured protein interaction pairs.

19.2.3. Tip and Sample Preparation

In studies of protein–protein interactions, the protein or ligand is immobilized on the surface of an AFM cantilever tip while its cognate binding partner is attached to a suitable substrate. After bringing the two surfaces into contact, the interaction force is acquired from the deflection of the cantilever during its withdrawal from the substrate. Therefore, proper tip and sample preparation is essential for the success of this type of study. The techniques commonly used to functionalize cantilevers involve either physisorption (13) or covalent coupling of the ligand to the tip via an extended linker (17). The linker between the tip and the ligand lends greater mobility and access to receptors on the surface being probed. Figure 19.3 outlines both methods for functionalizing tips.

Similar to tip functionalization, samples may be immobilized to surfaces by using physisorption or covalent coupling methods. Mica, polystyrene, and glass are widely used substrates for physisorption of proteins. Commonly used covalent coupling methods include thiol surface chemistry after gold deposition and cross-linking molecules of interest with a silanized surface.

Although the protocols for tip and surface functionalization are well established, one should bear in mind that coupling efficiency varies among different types of cantilevers or

Table 19.1. Summary of reported atomic force microscope unbinding studies

Ligand–Receptor Pair	Loading Rate (pN/sec)	Rupture forces (pN)	Barrier width (Å)	Ref.
$\alpha_5\beta_1$/fibronectin	50–50,000	40–170	0.9, 4	27
Aptamer/IgE	12,000–1,700,000	50–190	0.91, 2.54	53
Avidin-biotin	0.05–60,000	5–170	1.2, 3, 30	25
Azurin/cytochrome c551	7,000–150,000	50–150	1.4	54
Con A/D-mannose	400–5000	80–125	2.7	32
Digoxigenin/antibody	30–63,000	20–80	0.35, 1.15	55
GTPase Rap/impβ	300–80,000	40–90, 75–160[1]	N/A	30
LFA-1/ICAM-1	50–50,000	20–320	0.2, 2	26
LFA-1/ICAM-2	50–60,000	20–120	0.31–4.5	40
L-Selectin/PSGL-1[2]	10–100,000	20–160	0.6, 4	24
L-Selectin/sLeX[2]	10–100,000	10–180	0.6, 4	24
Mannuronan/AlgE 4	300–30,000	73–144	2.3	56
p53/azurin	3 nN/s	70	N/A	57
PDZ domain/peptide	3,800–140,000	40–220	0.4, 2.1	58
Plant lectin/asialofetuin	100–30,000	37–65	4–6	59
P-Selectin/PSGL-1	–[3]	110–170	2.5	60
P-selectin/PSGL-1	100–10,000	30–220	1.4	61
P-selectin/sLeX	70–100,000	20–220	0.8, 4.5	28
SfiI/DNA	2,100–630,000	25–100	1.8	62
Streptavidin–biotin	0.05–60,000	5–170	1.2, 5	25
TGF-β-1/receptor	100–13,000	40–200	0.73, 2.93	63
Transferrin(holo)/receptor	400–70,000	40–140	1.5, 9.3	29
Transferrin(apo)/receptor	500–40,000	25–40	8.1	29
VE-cadherin pair	–[3]	30–50	5.9	64
VLA-4/VCAM-1 (WT)	30–200,000	15–130	1, 5.5	65
VLA-4/VCAM-1 (D40A)	300–100,000	25–70	5.9	65
VLA-4/VCAM-1 (Q38G)	200–100,000	25–100	1.7, 5.8	65
VLA-4/VCAM-1 (L43K)	200–100,000	20–100	1.5, 5.7	65
VLA-4/VCAM-1 (D143A)	300–200,000	25–140	0.95, 5.8	65
Anti-γ-GT/γ-GT	N/A	131 ± 44	N/A	66
Antiferritin/ferritin	N/A	49 ± 10	N/A	67
Anti-HSA/HSA	N/A	240 ± 48	N/A	68
Anti-βhCG/βhCG	N/A	100 ± 47	N/A	69
Glycoprotein csA pair	N/A	23 ± 8	N/A	37
GroEL pair	N/A	420 ± 100	N/A	70
ICAM-1/anti-ICAM-1	N/A	100 ± 50	N/A	34
Insulin pair	N/A	1,340–1,350	N/A	71
Meromyosin/actin	N/A	15–25	N/A	72
Ocular mucin pair	N/A	100–4,000	N/A	73

Table 19.1. (continued)

Ligand–Receptor Pair	Loading Rate (pN/sec)	Rupture forces (pN)	Barrier width (Å)	Ref.
Proteoglycan pair	N/A	40 ± 15	N/A	74
$\alpha_5\beta_1$/GRGDSP peptide	N/A	32 ± 2	N/A	31
$\alpha_v\beta_3$/Osteopontin	N/A	50 ± 2	N/A	31

Con A, concanavalin A; βhCG, β subunit of human chorionic gonadotropin; GRGDSP, Gly-Arg-Gly-Asp-Ser-Pro; γ-GT, γ-glutamyl-transpeptidase; GTP, guanosine triphosphate; HAS, heat-stable antigen; ICAM-1, -2, intercellular adhesion molecules 1 and 2; IgE, immunoglobulin E; impβ, nuclear import receptor importin β1; LFA-1, leukocyte function-associated antigen-1; N/A, not available; PSGL-1, P-selectin glycoprotein ligand-1; TGF-β-1, transforming growth factor beta 1; VCAM-1, vascular cell adhesion molecule-1; VLA-4, very late antigen-4.

[1]The authors reported two populations of unbinding forces, reflecting the existence of two conformation states in the Rap/impβ complexes.

[2]Studies using biomembrane force probe.

[3]The authors reported unbinding forces versus different pulling velocities; we were unable to convert the velocity to loading rates.

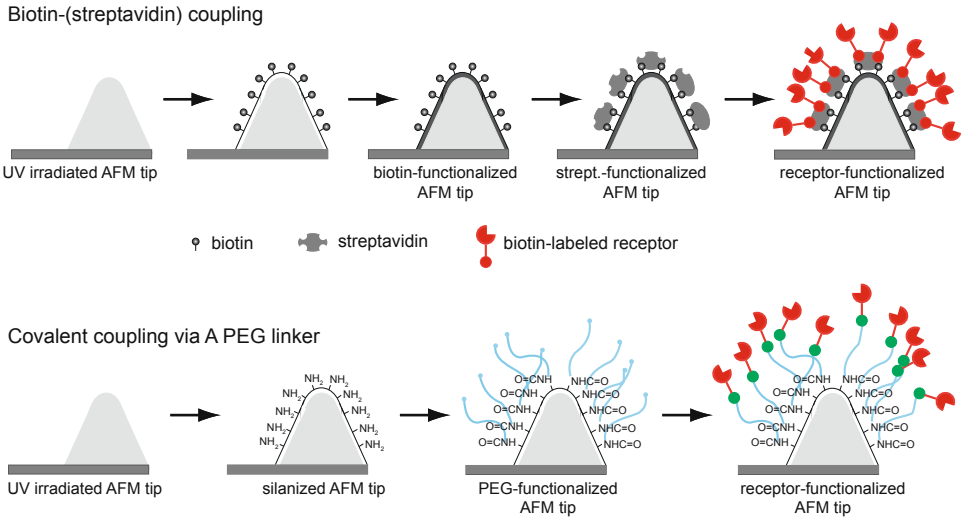

Figure 19.3. Schematics of surface chemistries commonly used for modifying atomic force microscope (AFM) tips. **A.** Functionalization of AFM tips with streptavidin using physisorption. **B.** Covalent coupling of proteins via a heterobifunctional poly(ethylene glycol) (PEG) cross-linker: The amine-reactive *N*-hydroxysuccinimide (NHS) end of the cross-linker reacts with amines on the silicon tip, yielding a stable amide bond, and the reactive 2-[pyridyldithio]propionate (PDP) group forms a bond with free thiols presented by cysteines in the protein, resulting in a stable disulfide bond. UV, ultraviolet.

surfaces, as well as among different molecules of interest. Thus, before performing force measurements, a detailed validation of the quality of functionalized tips and coupled samples is strongly recommended.

19.3. Determination of the Energy Landscape from the AFM Measurements

An AFM unbinding measurement (Figure 19.2) reveals the force required to break a ligand–receptor bond under a constant retraction velocity of the piezoelectric translator. For most of the measurement, the tension applied to break the bond increases linearly with time. The rate of change in tension, $rf = df/dt$, is known as the "loading rate" and can be experimentally controlled by varying the cantilever retraction velocity and/or the spring constant of the cantilever. For many ligand–receptor interactions, the unbinding force has been shown to change as the loading rate varies. In these studies, dependence of the unbinding forces on the measured loading rate can be used to reveal the energy landscape of the ligand–receptor complex.

The theoretical framework for understanding how a pulling force affects the dissociation of a protein–protein complex was first formulated by Bell in 1978 (18) and later expanded on by Evans and other researchers (19). Although recent refinements and generalizations have been developed (20–22), the Bell–Evans model can be seen as a first approximation to determining the energy landscape properties. The Bell–Evans model describes the influence of an external force on the rate of bond dissociation. This model is based on the conventional transition-state theory, in which a molecular complex needs to overcome an activation energy barrier before final separation. If only a single barrier dominates the dissociation process, the dissociation rate of this interaction is given by

$$k_{\text{off}} = \alpha \frac{k_{\text{B}}T}{h} \exp\left(\frac{-\Delta G^0}{k_{\text{B}}T}\right) \tag{19.1}$$

where ΔG^0 is the activation energy, T is the absolute temperature, k_{B} is Boltzmann's constant, h is Planck's constant, and α is a prefactor that characterizes the energy potential well. When the complex is exposed to a pulling force, the applied force adds a $-fx$ term to the potential of the system. If the potential barrier is steep, adding this term to the free energy reduces the activation barrier by approximately $f\gamma$, where γ is the width between the bound state and the transition state along the reaction coordinate. Thus, the force-dependent dissociation rate of the complex is given by

$$k_{\text{off}}(f) = \alpha \frac{k_{\text{B}}T}{h} \exp\left(\frac{-(\Delta G^0 - f\gamma)}{k_{\text{B}}T}\right) = k^o \exp\left(\frac{f\gamma}{k_{\text{B}}T}\right) \tag{19.2}$$

where k^o is the unstressed dissociation rate. Hence, the model predicts that the dissociation rate of the complex increases exponentially with a pulling force. The two parameters k^o and γ are often referred to as the Bell model parameters. These two parameters characterize the energy potential of the protein–protein complex. The depth of the potential is characterized by k^o, and γ characterizes the width of the potential and dictates the force resistance of a molecular complex. If a complex has a small γ (i.e., the activation potential is narrow), then an external force will have less effect on its force-dependent dissociation rate $k_{\text{off}}(f)$. On the other hand, if the activation potential is wide, the complex will be more sensitive to an external force because $f\gamma$ adds a larger term to the intermolecular potential.

Equation (19.2) describes how bond dissociation is changed by a constant pulling force. However, a constant pulling force is difficult to maintain in an AFM experiment. Instead, a dynamic force approach is generally used to characterize the forced dissociation

of ligand–receptor complexes (19,23). Under conditions of constant loading rate r_f, the probability density function for the forced unbinding of an adhesion complex is given by

$$P(f) = k^o \exp\left(\frac{\gamma f}{k_B T}\right) \exp\left\{\frac{k^o k_B T}{\gamma r_f}\left[1 - \exp\left(\frac{\gamma f}{k_B T}\right)\right]\right\} \tag{19.3}$$

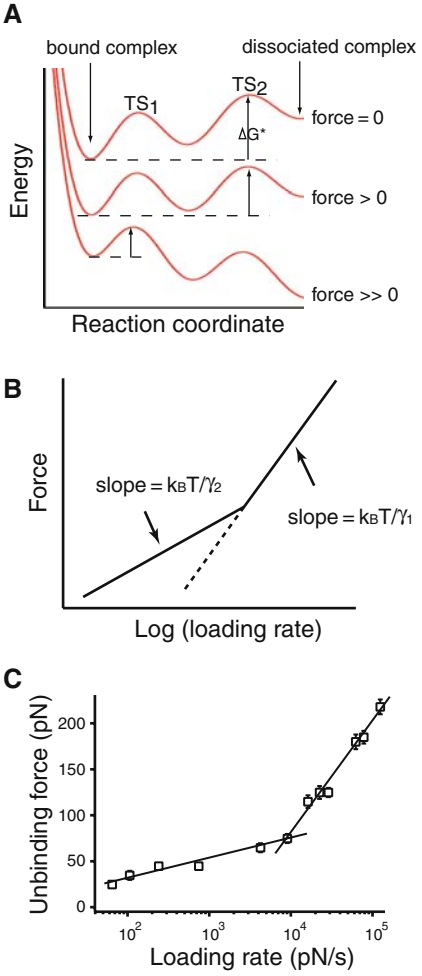

Figure 19.4. Dynamic force spectroscopy. **A.** Effects of an applied force on a protein–protein interaction potential consisting of two transition states, TS1 and TS2. In the absence of an applied force (*top*), the dissociation kinetics of the complex is determined by the outer energy barrier (i.e., TS2). An external force tilts the energy potential and suppresses the outer barrier (*middle*). Further increase in force results in a potential that is governed by the properties of the inner energy barrier (i.e., TS1) (*bottom*). **B.** Two linear regimes are predicted for a cascade of two sharp energy barriers. The increase of slope indicates that the outer barrier has been suppressed and the inner barrier has become the dominant kinetic impedance to detachment. **C**. Dynamic force spectra of the P-selectin/sLeX interactions (28). The best-fit curves (*solid lines*) were obtained using Eq. (19.4) applied to each of the two loading regimes. Error bars are the standard error of the mean (SEM). Some error bars are smaller than the symbols.

From (19.4), the most probable unbinding force f^* [i.e., the maximum of the distribution $\partial P(f)/\partial f = 0$] is

$$f^* = \frac{k_B T}{\gamma} \ln\left(\frac{\gamma}{k^o k_B T}\right) + \frac{k_B T}{\gamma} \ln(r_f) \tag{19.4}$$

Equation (19.4) shows that f^* is a linear function of the logarithm of the loading rate. The Bell model parameters are obtained from the plot of f^* versus $\ln(r_f)$, the dynamic force spectrum (DFS) of the complex (19).

The energy landscape of a complex may consist of multiple sharp activation barriers (Figure 19.4A) (19,23). In this case, the DFS is predicted to have multiple linear regimes with ascending slopes, as shown in Figure 19.2B. The increase in slope from one regime to the next indicates that an outer barrier has been suppressed by force and that an inner barrier dominates the dynamic response of the complex (Figure 19.3A). This theory is supported by recent experiments from different groups (24–27). Multiple activation barriers were found in a number of protein–protein systems, including the (strep)avidin/biotin complexes and all tested integrin/ligand complexes. A partial list of these studies is tabulated in Table 19.1.

19.4. Recent Applications

The following sections present some noteworthy and recent progress in using the AFM for protein–protein interaction studies.

19.4.1. Molecular Basis for Multiple Energy Barriers along with Protein–Protein Dissociation

Hundreds of protein pairs have been studied using the AFM. With the DFS approach, the dissociation of many protein complexes has been found to involve one or multiple potential energy barriers (Table 19.1). Recent experiments using site-directed mutagenesis and/or different physiological conditions have yielded important insight into the molecular and structural components that make up these energy barriers. This section highlights three studies investigating the molecular basis of protein interactions, with applications ranging from leukocyte extravasation, to iron transport, to receptor-mediated transport between the nucleus and cytoplasm.

The interaction between $\alpha_4\beta_1$ and vascular cell adhesion molecule-1 (VCAM-1) critically mediates leukocyte adhesion onto the vascular endothelium, and this interaction exhibits remarkable mechanical strength in resisting the large shear forces imposed by the bloodstream. To understand the molecular basis by which the $\alpha_4\beta_1$/VCAM-1 complex resists a pulling force, we employed single-molecule DFS to reveal that the dissociation of the $\alpha_4\beta_1$/VCAM-1 complex involves at least two activation potential barriers: a steep inner barrier granting the complex tensile strength to withstand large pulling forces (>50 pN) and a more elevated outer barrier that is stabilized by integrin activation (Table 19.1) (28). This special kinetic profile may reflect a biophysical basis permitting a dual physiological function (i.e., cell rolling and firm adhesion) of the $\alpha_4\beta_1$/VCAM-1 interaction. To correlate such features in the dissociation potential with molecular determinants, site-directed mutagenesis was applied to VCAM-1. Both using Mg^{2+} ion chelation and mutating Asp40 to the neutral residue alanine (D40A) suppressed the unbinding forces of the $\alpha_4\beta_1$/VCAM-1 complex, supporting the hypothesis that the inner barrier in the $\alpha_4\beta_1$/VCAM-1interaction is largely due

to the interaction between the chelated Mg^{2+} ion of the β_1 domain and the Asp40 residue of VCAM-1, an electrostatic interaction implicated by previous biochemical studies as most crucial to the stabilization of the complex. Mutagenesis of other residues in the C-D loop of D1 of VCAM-1 yielded smaller unbinding forces in both the slow- and fast-loading regimes, suggesting that variation in the dynamic strength of C-D loop mutants is due to differing widths of the inner barrier. In contrast, mutations in the D2 of VCAM-1 suppressed the unbinding force in the slow-loading regime but had no effect on forces in the fast-loading regime, suggesting that D2 of VCAM-1 helps to stabilize the activation energy of the outer barrier of the $\alpha_4\beta_1$/VCAM-1 complex (Table 19.1) (28). These DFS studies of D1 and D2 mutants provide a molecular explanation for the functionally relevant kinetic properties of the $\alpha_4\beta_1$/VCAM-1 interaction.

Multiple energy barriers have also been implicated in interactions between the iron transporter protein transferrin (Tf) and its receptor (TfR). In most mammalian cells, Tf R binds iron-loaded Tf (holo-TF) and transports it to endosomes, where acidic pH favors iron release. After returning to the cell surface, iron-free Tf (apo-TF) dissociates from TfR. Using an AFM tip functionalized with holo-Tf or apo-TF to probe TfR on both mica and cell surfaces, Yersin et al. (29) revealed striking differences between holo-Tf–TFR and apo-Tf–TfR interactions. Consistent with the accepted model of TfR cycling, the forces necessary to unbind holo-TF and TfR were always stronger than the unbinding forces required for the apo-Tf–TfR interaction, and the apo-Tf–TfR interaction was found to be pH dependent. Moreover, DFS measurements indicated that the dissociation of holo-Tf–TfR complexes involves overcoming two energy barriers, whereas apo-Tf–TfR complex dissociation involves overcoming only one. These distinct energy landscapes support a model of different binding points for holo-Tf–TfR and apo-Tf–TfR interactions.

Single-molecule studies have also yielded insight into the functional control of receptor-mediated transport of macromolecules between the nucleus and cytoplasm. The small GTPase Ran regulates the assembly and disassembly of receptor–cargo complexes by binding to the nuclear import receptor importin β1 (impβ) in its guanosine triphosphate (GTP)–bound form. Release of Ran from impβ is induced by effector proteins; however, it is unknown whether this change in stability is effected through an induced fit model whereby ligand binding triggers structural alterations or through dynamic population shifts in which changes in protein function and properties result from redistributions of preexisting conformational substates in response to binding. Using DFS to measure unbinding forces between single Ran–impβ pairs, Nevo et al. (30) found that Ran-GDP forms a single, weak complex with impβ, whereas Ran associated with the nonhydrolyzable GTP analog GppNHp leads to two distinct bound states whose fractional occupancy can be altered by applying mechanical force. The RanQ69L mutant, known for its markedly lowered GTPase activity, yielded a similar force spectrum to the wild-type analog when loaded with GDP. However, the mutant gave rise to a unimodal distribution of rupture forces in its GTP-bound form, suggesting that only the lower-strength state is accessible to GTP-bond RanQ69L. These data support a model of allosteric interactions regulating dynamic shifts between preexisting conformational isomers, extending the concept of multiple conformational states to macromolecular complexes.

19.4.2. AFM Measurements on Living Cells

Because the properties of purified molecules may not be the same as when they are in physiological conditions, it is best to study protein–protein interactions on living cells. However, the surface of a living cell is far more complicated than that of a bead or of mica coated

with protein. Furthermore, the low density of receptors on the cell surface and its nonspecific interactions introduce additional challenges. Lehenkari and Horton (31) were able to measure RGD (arginine-glycine-aspartic acid)-integrin binding on the surface of osteoblasts and osteoclasts, and we measured the binding force between concanavalin A and its receptor on the surface of NIH-3T3 fibroblasts (32).

Recent experiments in affinity imaging point to promising directions for studying protein–protein interactions with the AFM. Affinity imaging combines the force measurements of ligand–receptor interaction with the imaging function of the AFM. When the cantilever tip is coated with a specific protein, the AFM can provide an adhesion map detailing the density of the binding partner on a surface (33). Affinity images of antigens immobilized on a substrate were obtained using antibody-functionalized cantilevers (34). This technique has been extended to cell surfaces. Based on the specific interaction between *Helix pomatia* lectin and group A red blood cell plasma membrane proteins, Grandbois et al. (35) were able to discriminate group A from group O red blood cells. Similarly, the Dufrene group mapped numerous cell surface molecules on living bacteria (36).

The AFM has also been adapted for cell–cell adhesion studies (37,38). These experiments differed from those discussed earlier, in that a cell was attached to the end of the cantilever and used as a probe in cell adhesion studies. This approach allowed the study of both the ligand and the receptor under conditions close to their native environment. Potential applications of this approach include the study of modulated adhesion following cell activation. An example of such experiments is shown in Figure 19.5, in which a single leukocyte was attached to a concanavalin-A–functionalized cantilever. Using this protocol, we were able to measure the unbinding force of individual integrin leukocyte function–associated antigen-1 (LFA-1)/ICAM-1 (28,39,40) and integrin α5β1/fibronectin (27) bonds. Several other groups have also reported studies on different types of cell–cell interactions (41,42).

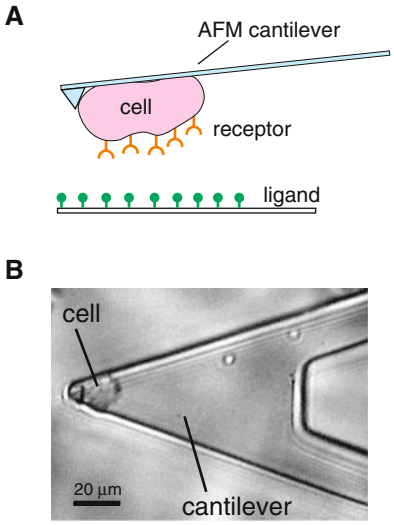

Figure 19.5. Study of protein–protein interactions in living cells. **A.** A live cell coupled to the atomic force microscope (AFM) cantilever. The cell expresses cell surface receptors, which will bind to the ligands immobilized on the tissue culture dish. **B.** Micrograph of a live leukocyte attached to the AFM cantilever. The bar is 20 μm.

19.4.3. Energy Landscape Roughness of Protein–Ligand Interaction

In its simplest representation, the energy landscape of molecular interactions between receptors and ligands is described by a barrier of certain height and width that determines the dissociation rate of the complex, as well as its dynamic strength. Some interactions, however, require a more complex landscape with additional barriers. Moreover, the surfaces of the energy landscape describing molecular interactions have been shown to be generally not smooth but to have varying heights that render them highly corrugated or rugged (43,44). This roughness slows down the dissociation kinetics of the interaction and contributes to its dynamic strength (45). Recently, it was shown that an estimate of the energy landscape roughness of protein–ligand interactions can be obtained from single-molecule dynamic force spectroscopy experiments conducted at different temperatures (46). These studies predicted that surface roughness increases the unbinding force of a protein–ligand complex at a given loading rate because it retards the unbinding process. As noted, the effect of surface roughness is temperature dependent, thus making it possible to estimate the energy roughness from AFM single-molecule measurements acquired at two temperatures T_1 and T_2. Specifically, the surface roughness ϵ of a protein–ligand interaction can be computed using Nevo's modification of the Hyeon and Thirumalai approximation,

$$\varepsilon^2 \approx \frac{x_\beta(T_1)k_\mathrm{B}T_1 x_\beta(T_2)k_\mathrm{B}T_2}{x_\beta(T_2)k_\mathrm{B}T_2 - x_\beta(T_1)k_\mathrm{B}T_1}\left[\Delta G^0\left(\frac{1}{x_\beta(T_1)} - \frac{1}{x_\beta(T_2)}\right) + \frac{k_\mathrm{B}T_1}{x_\beta(T_1)}\ln\frac{r_\mathrm{f}(T_1)x_\beta(T_1)}{k^o(T_1)k_\mathrm{B}T_1} - \frac{k_\mathrm{B}T_2}{x_\beta(T_2)}\ln\frac{r_\mathrm{f}(T_2)x_\beta(T_2)}{k^o(T_2)k_\mathrm{B}T_2}\right]$$

which takes into account the possible temperature dependence of the Bell model parameters $x_\beta(T)$ and $k^o(T)$ (45,46). Here, ΔG^0 is the height of the potential and $r_\mathrm{f}(T_1)$ and $r_\mathrm{f}(T_2)$ are the respective loading rates at the two different temperatures that give rise to the same unbinding force.

Using this approach, we recently obtained energy roughness values of $\sim 5.6 k_\mathrm{B}T$ and $7.5 k_\mathrm{B}T$ for the inner and outer barriers of the streptavidin–biotin complex, respectively (47). Similar values have been obtained for other systems, such as the unbinding of GTPase Ran from its receptor importin-β ($5.7 k_\mathrm{B}T$), the unbinding of complementary DNA strands ($10 k_\mathrm{B}T$), and the unfolding of the transmembrane helices of bacteriorhodopsin ($4 k_\mathrm{B}T$ to $6 k_\mathrm{B}T$) (46,48,49). In addition, when a force clamp technique was used to measure the unfolding rate of ubiquitin, Brujic et al. obtained a power-law distribution of unfolding rates that could be explained by assuming an exponential distribution of energy barriers with mean value of $6.6 k_\mathrm{B}T$ (50). The similarity in the results on such dissimilar systems suggests the possibility of a common origin for the roughness, perhaps due to the oversimplification involved in reducing the tridimensional dissociation pathway into a single reaction coordinate.

19.5. Concluding Remarks

Although the AFM is under improvement to enhance sensitivity (4), the major challenge for AFM research may stem from its availability, which is restricted to a limited number of laboratories. With the completion of various genome projects (including mapping the human genome, as well as the genomes of other animals and of plants), many gene sequences have been revealed. However, the proteins that genes encode do most of the work, such as building cells and running living organisms (51). Understanding how proteins interact with each other is a new frontier that may provide important insights into a variety of disease processes (52).

In the future, an AFM-based force spectroscopy approach will become increasingly important to elucidating the biophysical properties of many more protein–protein complexes. This methodology will also be increasingly adapted by biologists from different fields.

Acknowledgments

We are grateful for support by the National Institutes of Health (GM55611 to VTM), the American Heart Association (0215139B to XZ), the Fulbright-Generalitat de Catalunya postdoctoral fellowship (to FR) and the Harvard Medical School Medical Scientist Training Program fellowship (to AJX)

References

1. Wennmalm, S., and S. M. Simon. 2007. Studying individual events in biology. Annual Review of Biochemistry 76:419–446.
2. Greenleaf, W. J., M. T. Woodside, and S. M. Block. 2007. High-resolution, single-molecule measurements of biomolecular motion. Annual Review of Biophysics and Biomolecular Structure 36:171–190.
3. Binnig, G., C. F. Quate, and C. Gerber. 1986. Atomic force microscope. Physical Review Letters 56:930–933.
4. Horber, J. K., and M. J. Miles. 2003. Scanning probe evolution in biology. Science 302:1002–1005.
5. Lodish, H. F., A. Berk, P. Matsudaira, C. Kaiser, M. Krieger, M. Scott, L. Zipursky, and J. E. Darnell. 2004. Molecular Cell Biology, 5th ed. Scientific American Press, N.Y.
6. Barkai, E., Y. J. Jung, and R. Silbey. 2004. Theory of single-molecule spectroscopy: Beyond the ensemble average. Annual Review of Physical Chemistry 55:457–507.
7. Bustamante, C., J. C. Macosko, and G. J. L. Wuite. 2000. Grabbing the cat by the tail: Manipulating molecules one by one. Nature Reviews Molecular Cell Biology 1:130–136.
8. Orsello, C. E., D. A. Lauffenburger, and D. A. Hammer. 2001. Molecular properties in cell adhesion: A physical and engineering perspective. Trends in Biotechnology 19:310–316.
9. Bustamante, C., Y. R. Chemla, N. R. Forde, and D. Izhaky. 2004. Mechanical processes in biochemistry. Annual Review of Biochemistry 73:705–748.
10. Sader, J. E., I. Larson, P. Mulvaney, and L. R. White. 1995. Method for the calibration of atomic-force microscope cantilevers. Review of Scientific Instruments 66:3789–3798.
11. Senden, T. J., and W. A. Ducker. 1994. Experimental-determination of spring constants in atomic-force microscopy. Langmuir 10:1003–1004.
12. Hutter, J. L., and J. Bechhoefer. 1993. Calibration of atomic-force microscope tips. Review of Scientific Instruments 64:1868–1873.
13. Florin, E. L., V. T. Moy, and H. E. Gaub. 1994. Adhesion forces between individual ligand-receptor pairs. Science 264:415–417.
14. Alcaraz, J., L. Buscemi, M. Puig-de-Morales, J. Colchero, A. Baro, and D. Navajas. 2002. Correction of microrheological measurements of soft samples with atomic force microscopy for the hydrodynamic drag on the cantilever. Langmuir 18:716–721.
15. Janovjak, H., J. Struckmeier, and D. J. Muller. 2005. Hydrodynamic effects in fast AFM single-molecule force measurements. European Biophysics Journal with Biophysics Letters 34:91–96.
16. Lee, G. U., D. A. Kidwell, and R. J. Colton. 1994. Sensing discrete streptavidin–biotin interactions with AFM. Langmuir 10:354–361.
17. Hinterdorfer, P. 2002. Molecular recognition studies using the atomic force microscope. Methods in Cell Biology 68:115–139.
18. Bell, G. I. 1978. Models for the specific adhesion of cells to cells. Science 200:618–627.
19. Evans, E., and K. Ritchie. 1997. Dynamic strength of molecular adhesion bonds. Biophysical Journal 72:1541–1555.
20. Dudko, O. K., G. Hummer, and A. Szabo. 2006. Intrinsic rates and activation free energies from single-molecule pulling experiments. Physical Review Letters 96:108101.
21. Friddle, R. W. 2008. Unified model of dynamic forced barrier crossing in single molecules. Physical Review Letters 100:138302.

22. Husson, J., and F. Pincet. 2008. Analyzing single-bond experiments: Influence of the shape of the energy landscape and universal law between the width, depth, and force spectrum of the bond. Physical Review E 77:026108.
23. Evans, E. A., and D. A. Calderwood. 2007. Forces and bond dynamics in cell adhesion. Science 316:1148–1153.
24. Evans, E., A. Leung, D. Hammer, and S. Simon. 2001. Chemically distinct transition states govern rapid dissociation of single L-selectin bonds under force. Proceedings of the National Academy of Sciences of the United States of America 98:3784–3789.
25. Merkel, R., P. Nassoy, A. Leung, K. Ritchie, and E. Evans. 1999. Energy landscapes of receptor–ligand bonds explored with dynamic force spectroscopy. Nature 397:50–53.
26. Zhang, X., E. Wojcikiewicz, and V. T. Moy. 2002. Force spectroscopy of the leukocyte function-associated antigen-1/intercellular adhesion molecule-1 interaction. Biophysical Journal 83:2270–2279.
27. Li, F., S. D. Redick, H. P. Erickson, and V. T. Moy. 2003. Force measurements of the alpha(5)beta(1) integrin–fibronectin interaction. Biophysical Journal 84:1252–1262.
28. Zhang, X., D. F. Bogorin, and V. T. Moy. 2004. Molecular basis of the dynamic strength of the sialyl Lewis X–selectin interaction. Chemphyschem 5:175–182.
29. Yersin, A., T. Osada, and A. Ikai. 2008. Exploring transferrin-receptor interactions at the single-molecule level. Biophysical Journal 94:230–240.
30. Nevo, R., C. Stroh, F. Kienberger, D. Kaftan, V. Brumfeld, M. Elbaum, Z. Reich, and P. Hinterdorfer. 2003. A molecular switch between alternative conformational states in the complex of Ran and importin beta1. Nature Structural Biology 10:553–557.
31. Lehenkari, P. P., and M. A. Horton. 1999. Single integrin molecule adhesion forces in intact cells measured by atomic force microscopy. Biochemical and Biophysical Research Communications 259:645–650.
32. Chen, A., and V. T. Moy. 2000. Cross-linking of cell surface receptors enhances cooperativity of molecular adhesion. Biophysical Journal 78:2814–2820.
33. Kienberger, F., A. Ebner, H. J. Gruber, and P. Hinterdorfer. 2006. Molecular recognition imaging and force spectroscopy of single biomolecules. Accounts of Chemical Research 39:29–36.
34. Willemsen, O. H., M. M. Snel, K. O. van der Werf, B. G. de Grooth, J. Greve, P. Hinterdorfer, H. J. Gruber, H. Schindler, Y. van Kooyk, and C. G. Figdor. 1998. Simultaneous height and adhesion imaging of antibody-antigen interactions by atomic force microscopy. Biophysical Journal 75:2220–2228.
35. Grandbois, M., W. Dettmann, M. Benoit, and H. E. Gaub. 2000. Affinity imaging of red blood cells using an atomic force microscope. Journal of Histochemistry and Cytochemistry 48:719–724.
36. Dufrene, Y. F. 2008. AFM for nanoscale microbe analysis. Analyst 133:297–301.
37. Benoit, M., D. Gabriel, G. Gerisch, and H. E. Gaub. 2000. Discrete interactions in cell adhesion measured by single-molecule force spectroscopy. Nature Cell Biology 2:313–317.
38. Razatos, A., Y. L. Ong, M. M. Sharma, and G. Georgiou. 1998. Molecular determinants of bacterial adhesion monitored by atomic force microscopy. Proceedings of the National Academy of Sciences of the United States of America 95:11059–11064.
39. Wojcikiewicz, E. P., X. Zhang, A. Chen, and V. T. Moy. 2003. Contributions of molecular binding events and cellular compliance to the modulation of leukocyte adhesion. Journal of Cell Science 116:2531–2539.
40. Wojcikiewicz, E. P., M. H. Abdulreda, X. H. Zhang, and V. T. Moy. 2006. Force spectroscopy of LFA-1 and its ligands, ICAM-1 and ICAM-2. Biomacromolecules 7:3188–3195.
41. Krieg, M., Y. Arboleda-Estudillo, P. H. Puech, J. Kafer, F. Graner, D. J. Muller, and C. P. Heisenberg. 2008. Tensile forces govern germ-layer organization in zebrafish. Nature Cell Biology 10:429–U122.
42. Puech, P. H., K. Poole, D. Knebel, and D. J. Muller. 2006. A new technical approach to quantify cell-cell adhesion forces by AFM. Ultramicroscopy 106:637–644.
43. Ansari, A., J. Berendzen, S. F. Bowne, H. Frauenfelder, I. E. T. Iben, T. B. Sauke, E. Shyamsunder, and R. D. Young. 1985. Protein states and protein quakes. Proceedings of the National Academy of Sciences of the United States of America 82:5000–5004.
44. Frauenfelder, H., S. G. Sligar, and P. G. Wolynes. 1991. The energy landscapes and motions of proteins. Science 254:1598–1603.
45. Hyeon, C., and D. Thirumalai. 2007. Measuring the energy landscape roughness and the transition state location of biomolecules using single molecule mechanical unfolding experiments. Journal of Physics—Condensed Matter 19:113101.
46. Nevo, R., V. Brumfeld, R. Kapon, P. Hinterdorfer, and Z. Reich. 2005. Direct measurement of protein energy landscape roughness. EMBO Reports 6:482–486.
47. Rico, F., and V. T. Moy. 2007. Energy landscape roughness of the streptavidin-biotin interaction. Journal of Molecular Recognition 20:495–501.
48. Janovjak, H., H. Knaus, and D. J. Muller. 2007. Transmembrane helices have rough energy surfaces. Journal of the American Chemical Society 129:246–247.

49. Schumakovitch, I., W. Grange, T. Strunz, P. Bertoncini, H. J. Guntherodt, and M. Hegner. 2002. Temperature dependence of unbinding forces between complementary DNA strands. Biophysical Journal 82:517–521.
50. Brujic, J., R. I. Hermans, K. A. Walther, and J. M. Fernandez. 2006. Single-molecule force spectroscopy reveals signatures of glassy dynamics in the energy landscape of ubiquitin. Nature Physics 2:282–286.
51. Walhout, A. J. M., and M. Vidal. 2001. Protein interaction maps for model organisms. Nature Reviews Molecular Cell Biology 2:55–62.
52. Wells, J. A., and C. L. McClendon. 2007. Reaching for high-hanging fruit in drug discovery at protein-protein interfaces. Nature 450:1001–1009.
53. Yu, J. P., Y. X. Jiang, X. Y. Ma, Y. Lin, and X. H. Fang. 2007. Energy landscape of aptamer/protein complexes studied by single-molecule force spectroscopy. Chemistry—An Asian Journal 2:284–289.
54. Bonanni, B., A. S. M. Kamruzzahan, A. R. Bizzarri, C. Rankl, H. J. Gruber, P. Hinterdorfer, and S. Cannistraro. 2005. Single molecule recognition between cytochrome C 551 and gold-immobilized azurin by force spectroscopy. Biophysical Journal 89:2783–2791.
55. Neuert, G., C. Albrecht, E. Pamir, and H. E. Gaub. 2006. Dynamic force spectroscopy of the digoxigenin–antibody complex. EBS Letters 580:505–509.
56. Sletmoen, M., G. Skjak-Braek, and B. T. Stokke. 2004. Single-molecular pair unbinding studies of mannuronan C-5 epimerase AlgE4 and its polymer substrate. Biomacromolecules 5:1288–1295.
57. Taranta, M., A. R. Bizzarri, and S. Cannistraro. 2008. Probing the interaction between p53 and the bacterial protein azurin by single molecule force spectroscopy. Journal of Molecular Recognition 21:63–70.
58. Maki, T., S. Kidoaki, K. Usui, H. Suzuki, M. Ito, F. Ito, Y. Hayashizaki, and T. Matsuda. 2007. Dynamic force spectroscopy of the specific interaction between the PDZ domain and its recognition peptides. Langmuir 23:2668–2673.
59. Dettmann, W., M. Grandbois, S. Andre, M. Benoit, A. K. Wehle, H. Kaltner, H. J. Gabius, and H. E. Gaub. 2000. Differences in zero-force and force-driven kinetics of ligand dissociation from beta-galactoside-specific proteins (plant and animal lectins, immunoglobulin G) monitored by plasmon resonance and dynamic single molecule force microscopy. Archives of Biochemistry and Biophysics 383:157–170.
60. Fritz, J., A. G. Katopodis, F. Kolbinger, and D. Anselmetti. 1998. Force-mediated kinetics of single P-selectin/ligand complexes observed by atomic force microscopy. Proceedings of the National Academy of Sciences of the United States of America 95:12283–12288.
61. Hanley, W., O. McCarty, S. Jadhav, Y. Tseng, D. Wirtz, and K. Konstantopoulos. 2003. Single molecule characterization of P-selectin/ligand binding. Journal of Biological Chemistry 278:10556–10561.
62. Krasnoslobodtsev, A. V., L. S. Shlyakhtenko, and Y. L. Lyubchenko. 2007. Probing interactions within the synaptic DNA-Sfil complex by AFM force spectroscopy. Journal of Molecular Biology 365:1407–1416.
63. Yu, J. P., Q. Wang, X. L. Shi, X. Y. Ma, H. Y. Yang, Y. G. Chen, and X. H. Fang. 2007. Single-molecule force spectroscopy study of interaction between transforming growth factor beta 1 and its receptor in living cells. Journal of Physical Chemistry B 111:13619–13625.
64. Baumgartner, W., P. Hinterdorfer, W. Ness, A. Raab, D. Vestweber, H. Schindler, and D. Drenckhahn. 2000. Cadherin interaction probed by atomic force microscopy. Proceedings of the National Academy of Sciences of the United States of America 97:4005–4010.
65. Zhang, X., S. E. Craig, H. Kirby, M. J. Humphries, and V. T. Moy. 2004. Molecular basis for the dynamic strength of the integrin alpha4beta1/VCAM-1 interaction. Biophysical Journal 87:3470–3478.
66. Wielert-Badt, S., P. Hinterdorfer, H. J. Gruber, J. T. Lin, D. Badt, B. Wimmer, H. Schindler, and R. K. Kinne. 2002. Single molecule recognition of protein binding epitopes in brush border membranes by force microscopy. Biophysical Journal 82:2767–2774.
67. Allen, S., X. Chen, J. Davies, M. C. Davies, A. C. Dawkes, J. C. Edwards, C. J. Roberts, J. Sefton, S. J. Tendler, and P. M. Williams. 1997. Detection of antigen–antibody binding events with the atomic force microscope. Biochemistry 36:7457–7463.
68. Hinterdorfer, P., W. Baumgartner, H. J. Gruber, K. Schilcher, and H. Schindler. 1996. Detection and localization of individual antibody-antigen recognition events by atomic force microscopy. Proceedings of the National Academy of Sciences of the United States of America 93:3477–3481.
69. Allen, S., J. Davies, M. C. Davies, A. C. Dawkes, C. J. Roberts, S. J. Tendler, and P. M. Williams. 1999. The influence of epitope availability on atomic-force microscope studies of antigen-antibody interactions. Biochemical Journal 341:173–178.
70. Vinckier, A., P. Gervasoni, F. Zaugg, U. Ziegler, P. Lindner, P. Groscurth, A. Pluckthun, and G. Semenza. 1998. Atomic force microscopy detects changes in the interaction forces between GroEL and substrate proteins. Biophysical Journal 74:3256–3263.
71. Yip, C. M., C. C. Yip, and M. D. Ward. 1998. Direct force measurements of insulin monomer-monomer interactions. Biochemistry 37:5439–5449.

72. Nakajima, H., Y. Kunioka, K. Nakano, K. Shimizu, M. Seto, and T. Ando. 1997. Scanning force microscopy of the interaction events between a single molecule of heavy meromyosin and actin. Biochemical and Biophysical Research Communications 234:178–182.
73. Berry, M., T. J. McMaster, A. P. Corfield, and M. J. Miles. 2001. Exploring the molecular adhesion of ocular mucins. Biomacromolecules 2:498–503.
74. Dammer, U., O. Popescu, P. Wagner, D. Anselmetti, H. J. Guntherodt, and G. N. Misevic. 1995. Binding strength between cell adhesion proteoglycans measured by atomic force microscopy. Science 267:1173–1175.